

# A vortical phantom for ASL perfusion MRI

Aaron Oliver-Taylor<sup>1</sup> Xavier Golay<sup>1,2</sup>

<sup>1</sup>Gold Standard Phantoms Limited, London, United Kingdom,

<sup>2</sup>Institute of Neurology, University College London, London, United Kingdom

## 1. Introduction

- Despite standardisation of Arterial Spin Labelling implementations[1], it is challenging to demonstrate as a truly quantitative and calibrated measurement technique.
- Current reference standards are either based on independent measurements using a validated method such as <sup>15</sup>O-PET[2], or the use of phantoms.
- The majority of existing perfusion phantoms for ASL rely upon a distribution network and/or a porous medium to simulate the microvasculature[3-5].
- A recent new phantom design based on impinging jets[6] has shown to be able to simulate perfusion without the presence of a porous material.
- This removes the need to characterise the porous media, reducing the overall uncertainty associated with a perfusion measurement.
- Here, we investigate whether a commercially available perfusion phantom[5] can be adapted to this concept.

## 3. MRI Acquisition

- 3T MRI system (Achieva dStream, Philips Healthcare) running software version R5.4.0.
- Time of Flight (TOF) angiogram of the entire perfusion chamber.
- Single-slice sagittal phase contrast velocimetry with flow weighting along all three axes,  $v_{enc} = 40\text{cm/s}$
- Minimal acquisition artefact, multi-PLD pCASL, 1.8 s label duration, PLD's ranging 0.8 to 2.4 s in 0.2 s increments:
  - Four 2D-EPI control-label pairs for each PLD,
  - 256 x 192 x 56 mm FOV, 4mm slice thickness, 2 x 2 mm in-plane resolution
  - Flow compensated, 28 x 96 acquisition matrix, EPI factor 7, SENSE factor 2.3, 8 shots per image.
  - 8.622 ms TE, 5 s TR, 260 s acquisition duration per PLD.
- MO with the same acquisition parameters as the ASL
- During the TOF, phase contrast, ASL and MO scans the phantom flow rate was set to 350ml/min.
- Single-slice sagittal inversion recovery for measuring T1, TI = 100, 300, 500, 1000, 2000, 3000 ms, TR = TI + TW, where TW = 2000ms, acquired with the phantom's pump off.

## 2. Phantom Design

- The 'perfusion unit' of the perfusion phantom comprises two chambers:
  - a 10cm diameter cylindrical 'labelling chamber' in which the inlet tube runs and is surrounded by doped water to provide proper B<sub>0</sub> homogeneity.
  - a 12cm diameter, 49.5mm diameter cylindrical 'perfusion chamber', connected to the inlet tube via a branching region where the flow splits into sixty 1mm wide channels.
- In the original commercial phantom the perfusion chamber would normally contain:
  - Six 4.75mm thick, 116mm diameter discs of sintered UHMW-PE, creating a 'block' of porous material to simulate the parenchyma
  - A 5mm thick disc of acetal to clamp against the porous discs.
  - A set of three rods with round nuts at one end to secure the porous and acetal discs in place.
- This was all removed, resulting in a 120mm diameter, 49.5mm deep cylindrical space fed by sixty 1mm diameter inlets.
- The perfusion unit was then filled with a standard water-based perfusate and connected as normal to the pump system.
- The pump system contains a calibrated optical turbine flow meter, with an accuracy of 1%. The flow rate is sampled at 10Hz, and as well as being recorded in real-time, a PID algorithm uses the measured flow rate in a PID control loop to maintain the flow rate at a prescribed setpoint.

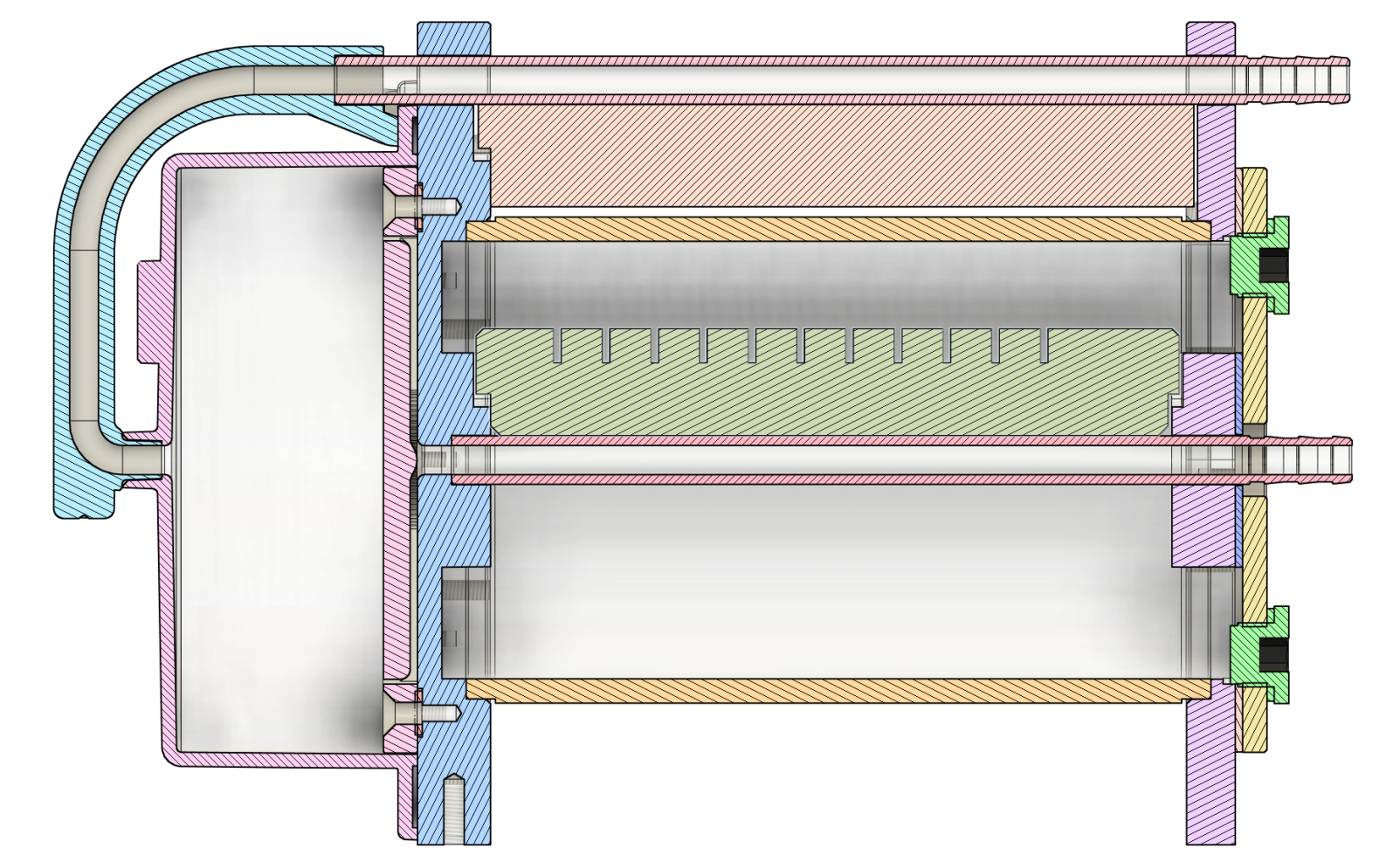


Figure 1. Cross section through the modified perfusion chamber.

## 4. Image Analysis

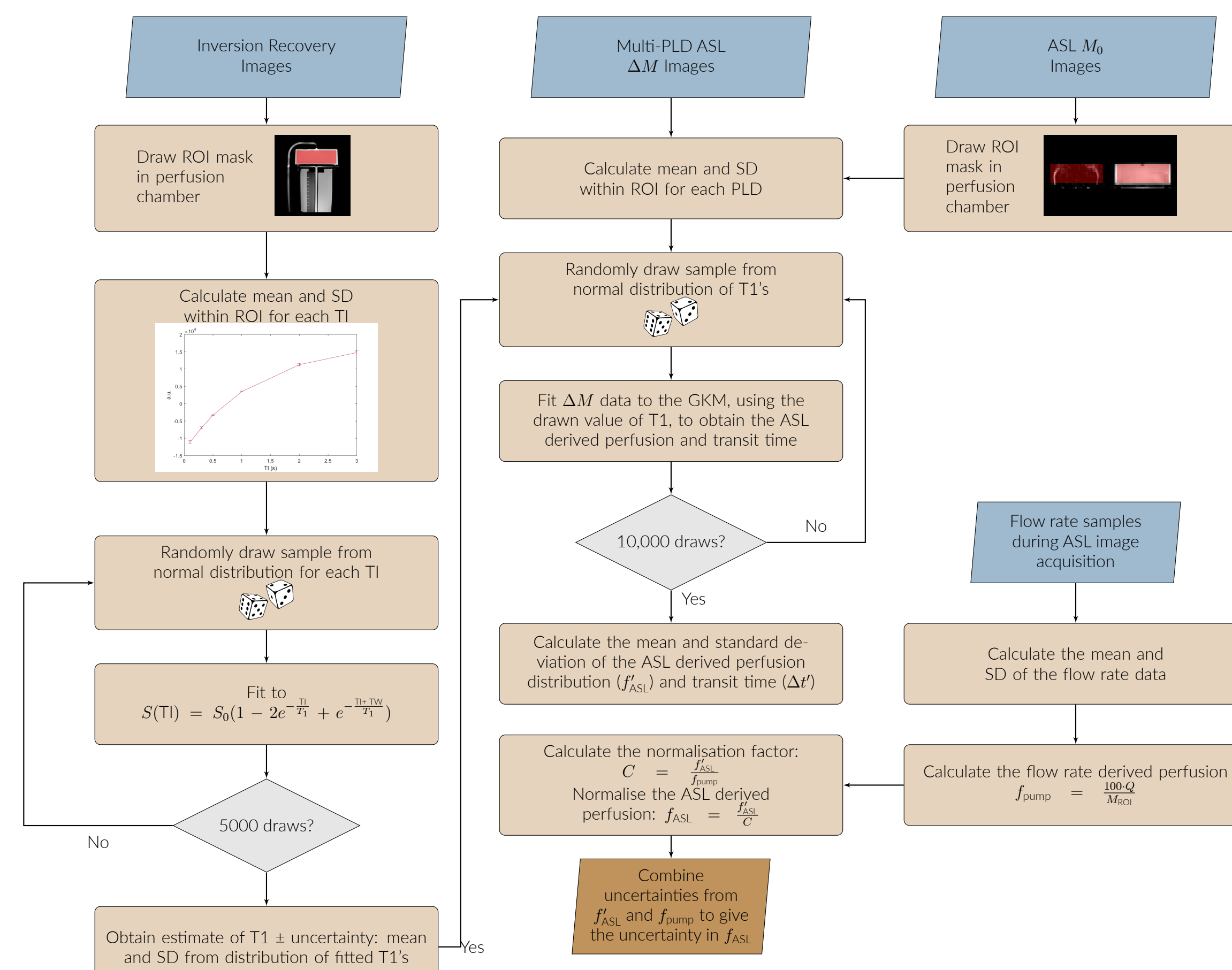


Figure 2. Analysis pipeline schematic

- Data were analysed using custom software developed in Matlab (R2016b, The Mathworks).
- DICOM images first were converted to NIFTI using dcm2nii[7] v1.0.20200331.
- ROI masks encompassing the perfusion chamber were drawn using itk-SNAP[8] then saved to NIFTI.
- $f_{ASL}$  and  $\Delta t$  were calculated by least-squares fit to the ASL General Kinetic Model[9, 10] using the randomly drawn value for both the tissue and blood T<sub>1</sub>, and assuming  $\lambda = 1.0\text{g/ml}$  and that the labelling efficiency is 100%.

## 5. Results

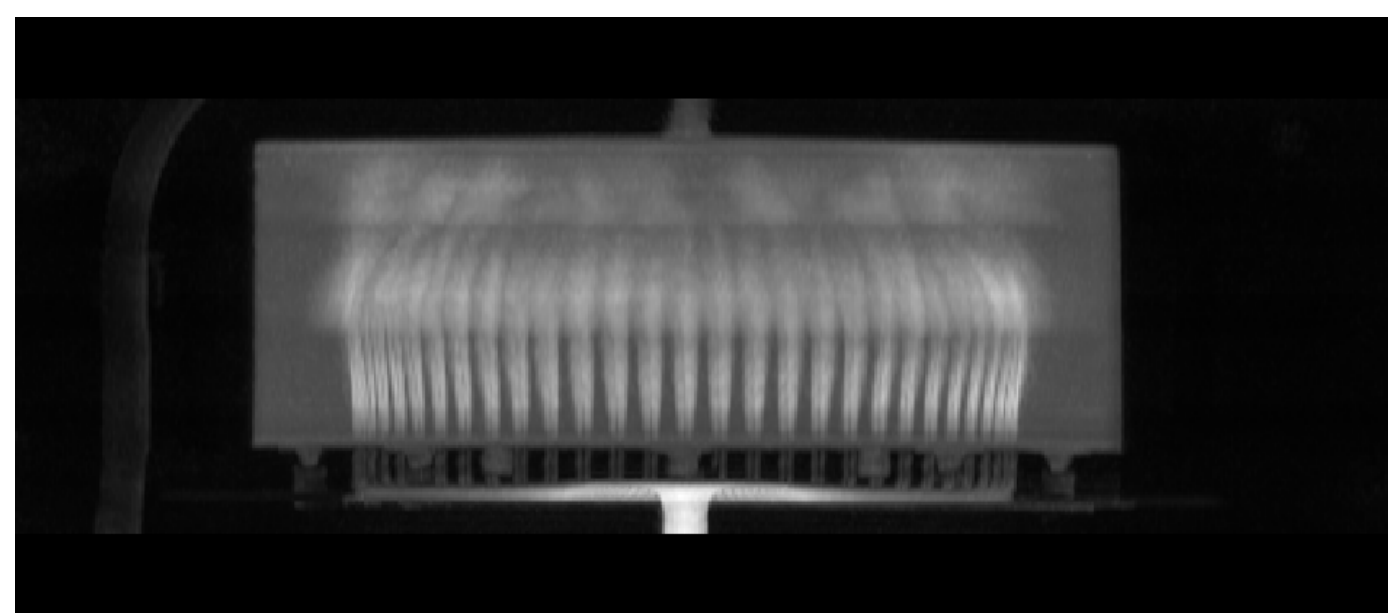


Figure 3. Sagittal maximum intensity projection (MIP) from the Time of Flight Angiogram. The inlet at the base of the image branches out to the 60 'arteriole' inlets which then travel into the perfusion chamber. Here they are at first individually defined, and then from about mid-way through the chamber begin to interfere and mix

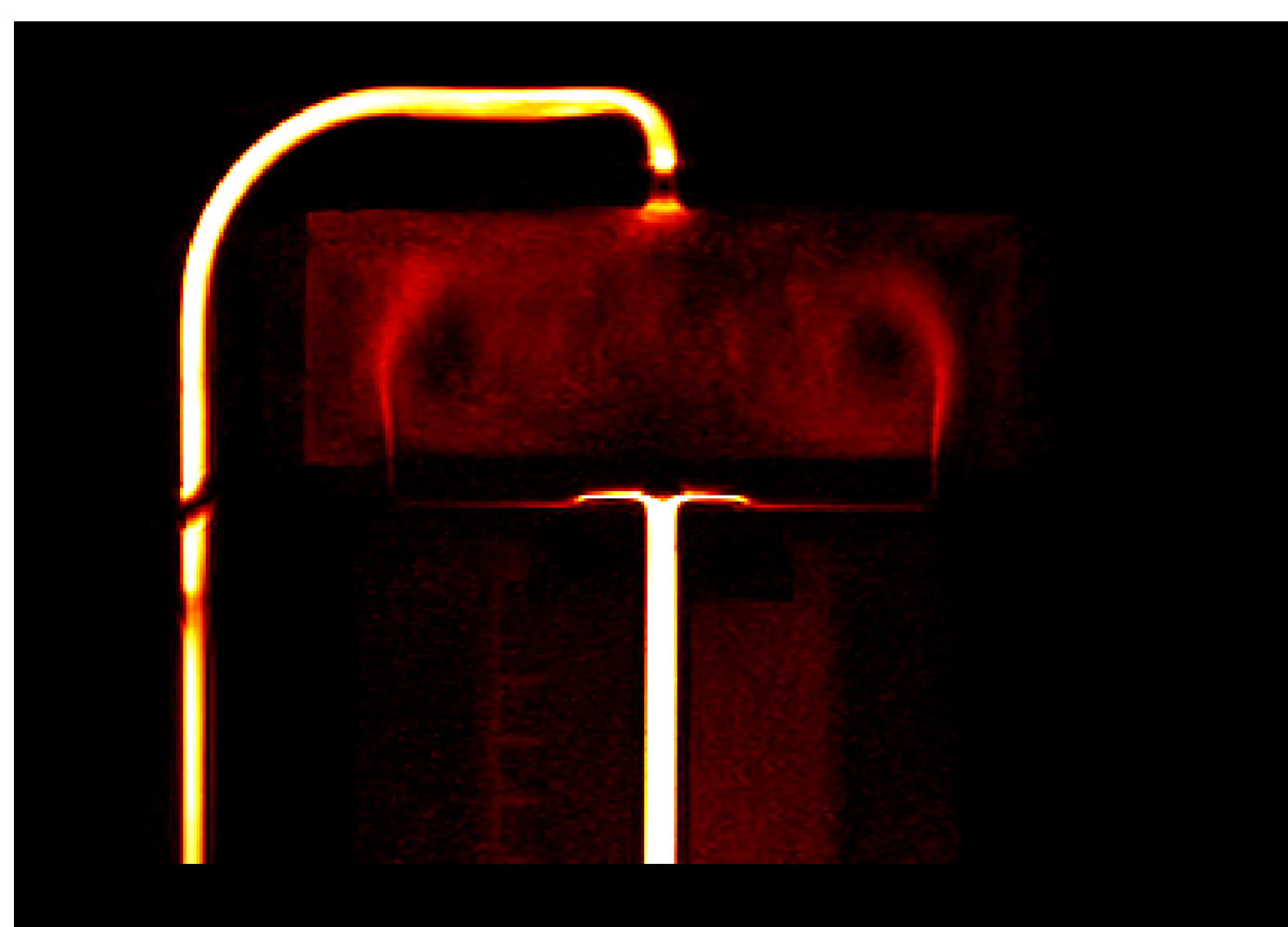


Figure 4. Phase contrast velocimetry image showing the calculated norm of the velocity vector in each voxel. The dark regions just inside the inlets are stationary zones within regions that recirculate perfusate within the chamber due to the established vortical flow.

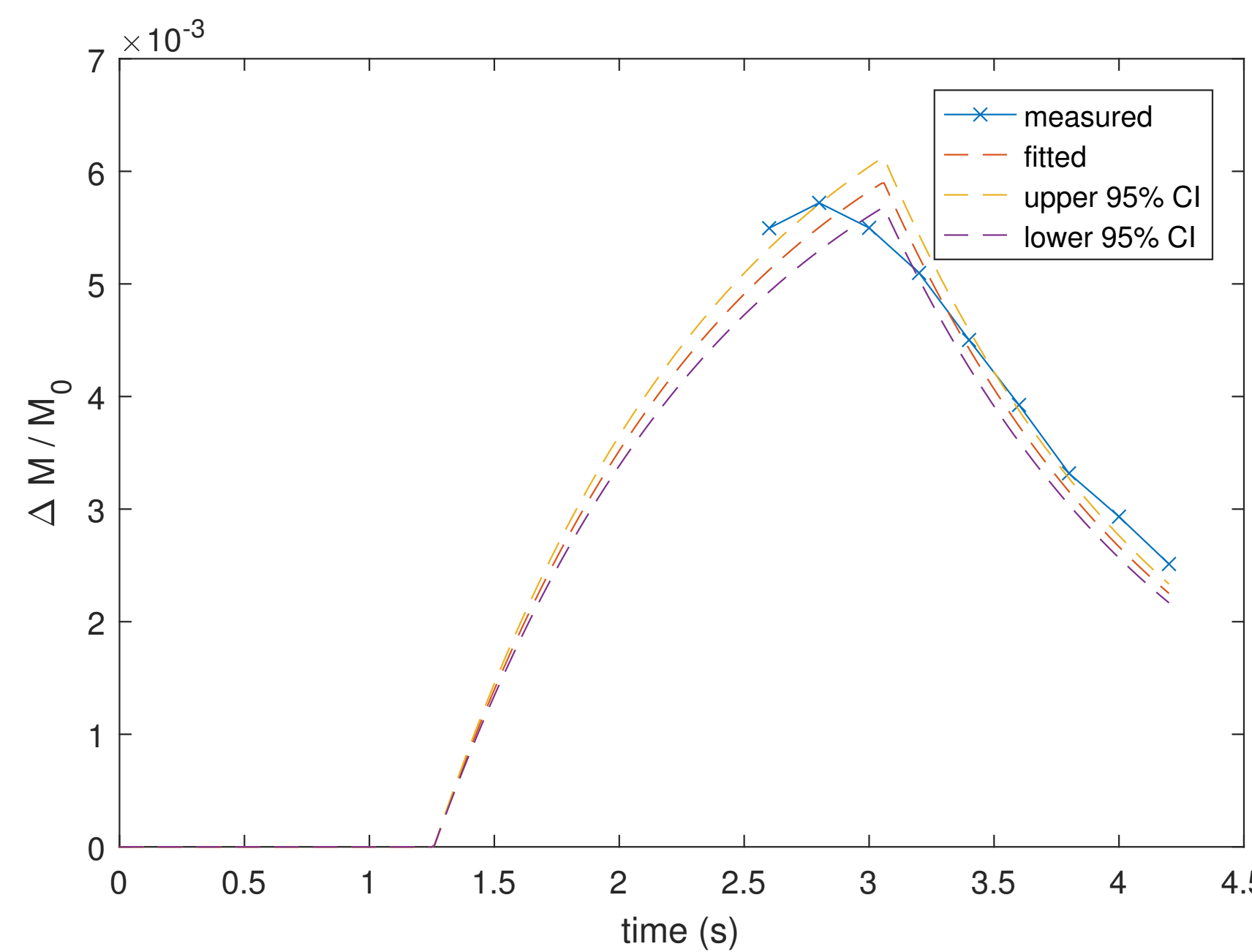


Figure 5.  $\frac{\Delta M}{M_0}$  signal curves since the onset of labelling, for the measured data (blue line) and a calculated curve based on the fitted values for perfusion rate and transit time, corrected using the normalisation constant (orange dashed line)

- The fitted T<sub>1</sub> values are shown in Figure 7, clearly showing a normal distribution. The estimated perfusate T<sub>1</sub> was  $1.20 \pm 0.02$  s.
- The pump flow rate during all acquisitions was  $350.00 \pm 4.87$  ml/min (mean  $\pm$  standard deviation in the measured flow rate, combined with the 1% accuracy of the flow meter), corresponding to a pump derived perfusion rate into the chamber of  $84.94 \pm 1.18$  ml/100g/min.
- Prior to normalisation the ASL derived perfusion was  $54.44 \pm 0.52$  ml/100g/min, with a uniform distribution of values (see Figure 8). After normalisation such that  $f_{ASL} \equiv f_{pump}$ , the uncertainty in the ASL derived perfusion was  $1.65$  ml/100g/min. The estimated transit time was  $1.26 \pm 0.002$  s.
- The normalisation factor  $C$  was  $0.641 \pm 0.011$ .
- The sum-of-squares error between measured and fitted curves was  $5.2 \times 10^{-7}$ .

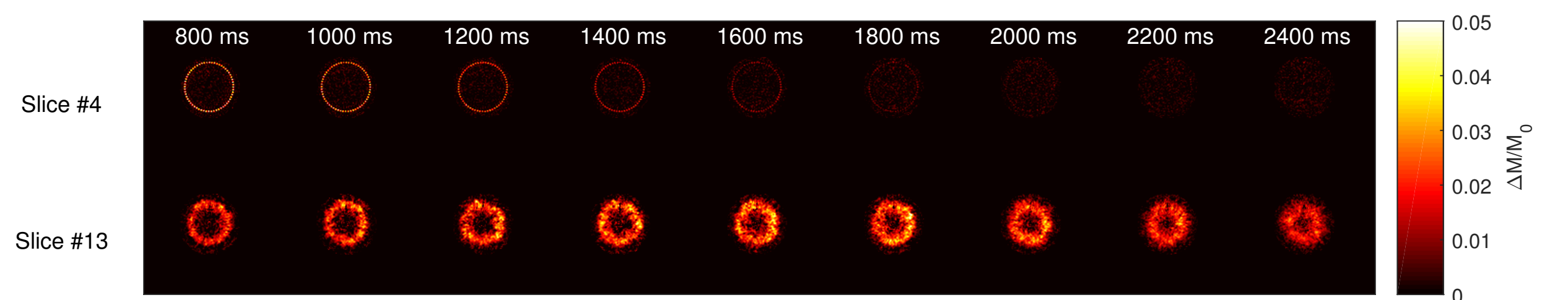


Figure 6.  $\frac{\Delta M}{M_0}$  images for a slice close to the inlets (slice #4) and outlet (slice #13) of the perfusion chamber. Even at a PLD of 2.4s signal has not yet left the perfusion chamber, as indicated by the hypointense region in the middle of slice #13.

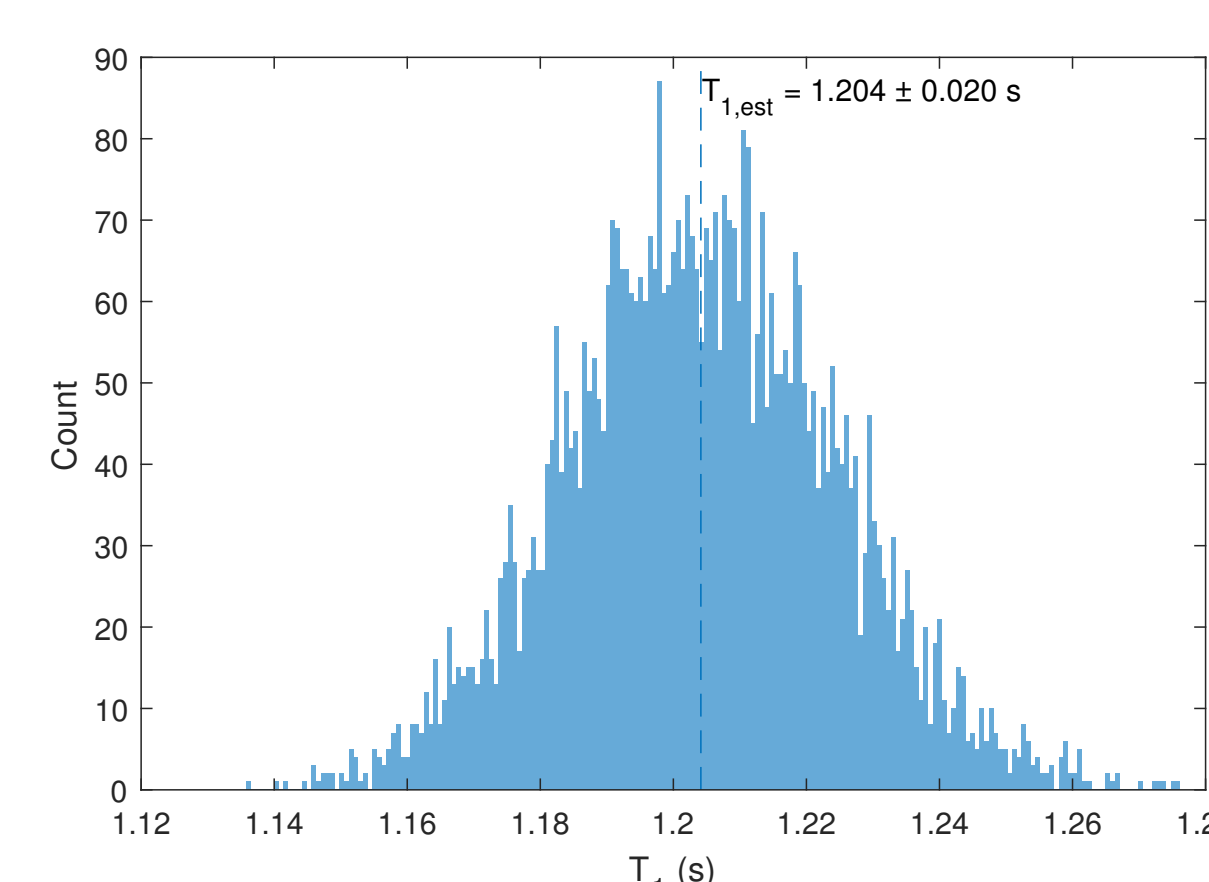


Figure 7. Histogram of the estimated T<sub>1</sub> values based on randomly drawing the inversion recovery signal for each TI based on the measured mean and standard deviations within the perfusion chamber ROI. The resultant distribution is clearly normal.

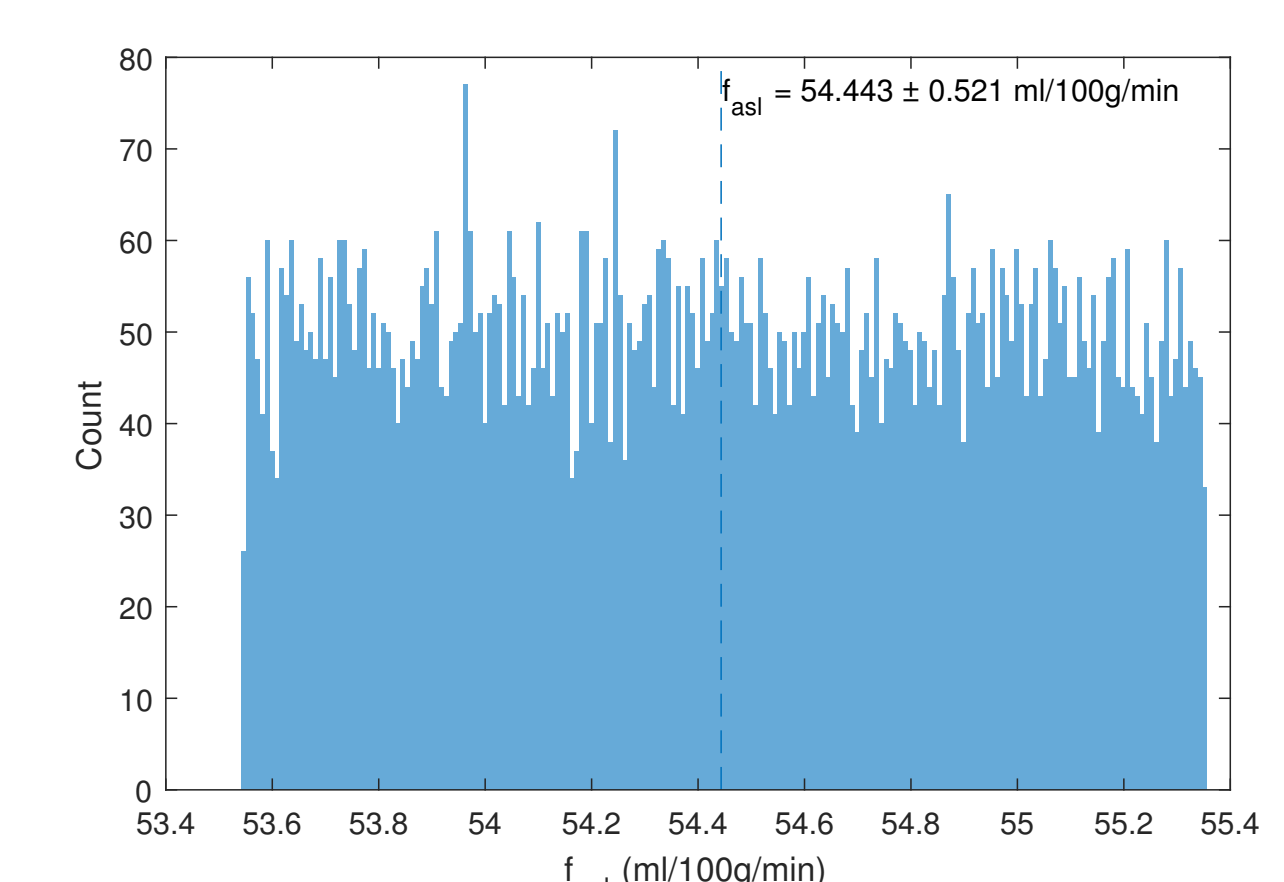


Figure 8. Histogram of the estimated perfusion values prior to normalisation based on randomly drawing T<sub>1</sub> based on the estimated mean and uncertainty in the perfusate T<sub>1</sub>.

## 6. Discussion

- Results indicate that it is possible to simulate perfusion without the need for porous media or impinging jets, utilising vortical mixing from multiple adjacent inlets.
- In comparison with human data[11], the calibrated flow measurement system within the phantom provides an independent ground truth for the system flow rate with known uncertainty.
- Due to clinical software restrictions it was not possible to acquire a full range of PLDs, which would improve this assessment.
- By equating the ASL derived and pump derived perfusions, the measured  $\Delta M$  data is in very good agreement with the predictions made by the general kinetic model.
- However, from Figure 5 it is evident that the measured data curve does not have the sharp discontinuity between rising and decaying segments, and decays with a longer time constant, possibly due to the approximation that the bolus has been completely delivered at  $\tau + \Delta t$ , whereas in practise the labelled bolus may experience some dispersion.
- The uncertainties associated with the T<sub>1</sub> measurement and the measurement of the system flow rate during all the ASL acquisitions can be propagated to give an overall uncertainty in the ASL derived perfusion measurement of 1.94%.
- A significant component of the normalisation coefficient will be the labelling efficiency. 0.64 is significantly lower than what would be expected for the velocities in the labelling tube (20 - 40 cm/s), so either the labelling efficiency was sub-optimal possibly due to poor shim, or there are other components that contribute to this normalisation constant. Independent measurements of the labelling efficiency at multiple flow rates would help to understand this further, and identify the other contributions.
- A phantom in which it is possible to equate measured perfusion with the systemic flow rate has great appeal:
  - Validation of new imaging methods[12].
  - A verification of labelling efficiency alongside independent measures of T<sub>1</sub> and  $\alpha$ .
  - Assessment of linearity between flow and measured ASL perfusion; demonstrating linearity between a quantitative imaging biomarker and its inputs which is a necessary step in establishing the claims of a QIBA[13] profile.
  - Routine quality assurance of ASL acquisitions.

## 7. Conclusions

- Presented is a perfusion phantom that demonstrates porous media-free perfusion.
- Without the need to characterise the porous media, we are able to simply equate the measured perfusion with the pump flow rate.
- Future work will include the acquisition of a fuller set of PLDs over a range of different pump flow rates, and to independently measure the labelling efficiency for verification.

## References

- Alsop, D. C.; Detre, J. A.; Golay, X.; Günther, M.; Hendrikse, J.; Hernandez-Garcia, L.; Lu, H.; MacIntosh, B. J.; Parkes, L. M.; Smith, M.; van Osch, M. J. P.; Wang, D. J. J.; Wong, E. C.; Zaharchuk, G. *Magnetic Resonance in Medicine* **2015**, *73*, 102-116.
- Fan, A. P.; Jahanshahi, H.; Holdsworth, S. J.; Zaharchuk, G. *Journal of Cerebral Blood Flow & Metabolism* **2016**, *36*, 842-861.
- Esparsa-Coss, E.; Wosik, J.; Narayana, P. A. *Magnetic Resonance Imaging* **2010**, *28*, 607-612.
- Stafford, R. B.; Langham, M. C.; Davis, S. V.; Lee, J.; Detre, J. A. *In Proc. Intl. Soc. Mag. Reson. Med.* **2017**, Milan, Italy, 2014, A4572.
- Oliver-Taylor, A.; Gonçalves, M.; Hampshire, T.; Davis, B.; Daga, P.; Evans, L.; Bainbridge, A.; Wheeler-Kingshott, C.; Sokolska, M.; Thornton, J.; Vita, E. D.; Golay, X. *In Proceedings of ISMRM* **2017**, 2017.
- Gabrielyan, M.; Tisdall, M. D.; Kammer, C.; Higgins, C.; Arratia, P. E.; Detre, J. A. *Magnetic Resonance in Medicine* **2021**, *86*, 1145-1158.
- Li, X.; Morgan, P. S.; Ashburner, J.; Smith, J.; Rorden, C. *Journal of Neuroscience Methods* **2016**, *264*, 47-56.
- Yushkevich, P. A.; Piven, J.; Hazlett, H. C.; Smith, R. G.; Ho, S.; Gee, J. C.; Gerig, G. *NeuroImage* **2006**, *31*, 1116-1128.
- Buxton, R. B.; Frank, L. R.; Wong, E. C.; Siewert, B.; Warach, S.; Edelman, R. R. *Magnetic Resonance in Medicine* **1998**, *40*, 383-396.
- Golay, X.; Oliver-Taylor, A.; Suzuki, Y.; Chappell, M. *In ESMRMB 2019 Congress*, Rotterdam, Netherlands, 2019, A1672.
- Aslan, S.; Xu, F.; Wang, P. L.; Uhl, J.; Yezhovath, U. S.; van Osch, M.; Lu, H. *Magnetic Resonance in Medicine* **2010**, *63*, 765-771.
- Xu, F.; Zhu, D.; Fan, H.; Lu, H.; Liu, D.; Li, W.; Qin, Q. *Magnetic Resonance in Medicine* **2021**, *86*, 1360-1368.
- QIBA: <https://www.rsna.org/research/quantitative-imaging-biomarkers-alliance>.



Author email: aaron.oliver-taylor@goldstandardphantoms.com